



Recovery of Lithium Ions From Salt Lakes Using Nanofibers Containing Zeolite Carriers

Tao Ding¹, Mianping Zheng^{1,2}, Suping Peng¹, Zhen Nie², Yuhan Lin^{1*} and Qian Wu^{2*}

¹College of Geoscience and Surveying Engineering, China University of Mining and Technology (Beijing), Beijing, China, ²MNR Key Laboratory of Saline Lake Resources and Environments, Institute of Mineral Resources, Chinese Academy of Geological Sciences, Beijing, China

OPEN ACCESS

Edited by:

Muhammad Wakil Shahzad,
Northumbria University,
United Kingdom

Reviewed by:

Fahad Noor,
University of Engineering and
Technology, Lahore, Pakistan
Muhammad Ahmad Jamil,
Northumbria University,
United Kingdom

*Correspondence:

Yuhan Lin
1406973096@qq.com
Qian Wu
wuqian0516@163.com

Specialty section:

This article was submitted to
Process and Energy Systems
Engineering,
a section of the journal
Frontiers in Energy Research

Received: 14 March 2022

Accepted: 13 May 2022

Published: 27 May 2022

Citation:

Ding T, Zheng M, Peng S, Nie Z, Lin Y
and Wu Q (2022) Recovery of Lithium
Ions From Salt Lakes Using Nanofibers
Containing Zeolite Carriers.
Front. Energy Res. 10:895681.
doi: 10.3389/fenrg.2022.895681

Lithium is a key strategic metal in the 21st century and an important raw material in the new energy sector. With rapid growth of the market demand for lithium, the high-efficient extraction of lithium resources is of important economic significance. Taking zeolite as the carrier and using chemical grafting and electrospinning technologies, a kind of nanofiber containing crown ether (CE) was synthesized to adsorb Li(I) from the salt lake brine. This realizes the selective adsorption of Li(I) while retaining specific vacancies of epoxy groups in CE. The adsorption mechanism of nanofibers containing zeolite carriers and CE for Li(I) was revealed by the use of Fourier transform infrared (FT-IR) spectrometry, scanning electron microscopy (SEM), X-ray photoelectron spectroscopy (XPS), and density functional theory (DFT). The results show that after dsp^3 hybridization of the outer orbit (2s) of Li(I), outer electrons on the nanofibers containing zeolite carriers and CE mainly migrate to the orbit for coordination with Li(I) thereat, thus realizing the capture of Li(I). The novel adsorbing material can reach adsorption equilibrium within 2.5 h and the adsorption kinetics for Li(I) conforms to the pseudo-second-order model and a maximum adsorption capacity of 8.6 mg/g. It can be found that the correlation coefficient fitted by Langmuir adsorption isotherm model is closer to 1, and the calculated maximum adsorption capacity is closer to the adsorption capacity obtained experimentally, therefore, it can be concluded that the adsorption process is more consistent with the Langmuir adsorption isotherm model, and the adsorption process can be regarded as monolayer adsorption. The adsorption capacity remains at 7.8 mg/g after 5 adsorption–desorption cycles, showing favorable stability and a strong ability to be regenerated. The research provides insights into the adsorption and recovery of Li(I) from the salt lake brine.

Keywords: Li(I) in salt lakes, zeolite carrier, adsorption, density functional theory, regenerability

INTRODUCTION

Lithium, the lightest alkali metal, has been used as the cathode materials of lithium batteries due to advantages including a high energy storage density and low self-discharge rate (Tarascon and Armand, 2001; Berecibar, 2019). In recent years, because of requirements set by environmental changes such as global warming and carbon cycling (Jiménez-de-la-Cuesta and Mauritsen, 2019; Johnson and Lyman, 2020), the new energy industry dominated by lithium batteries has flourished (Lee et al., 2018; Wu et al., 2019), which calls for an increasing amount of lithium on the market

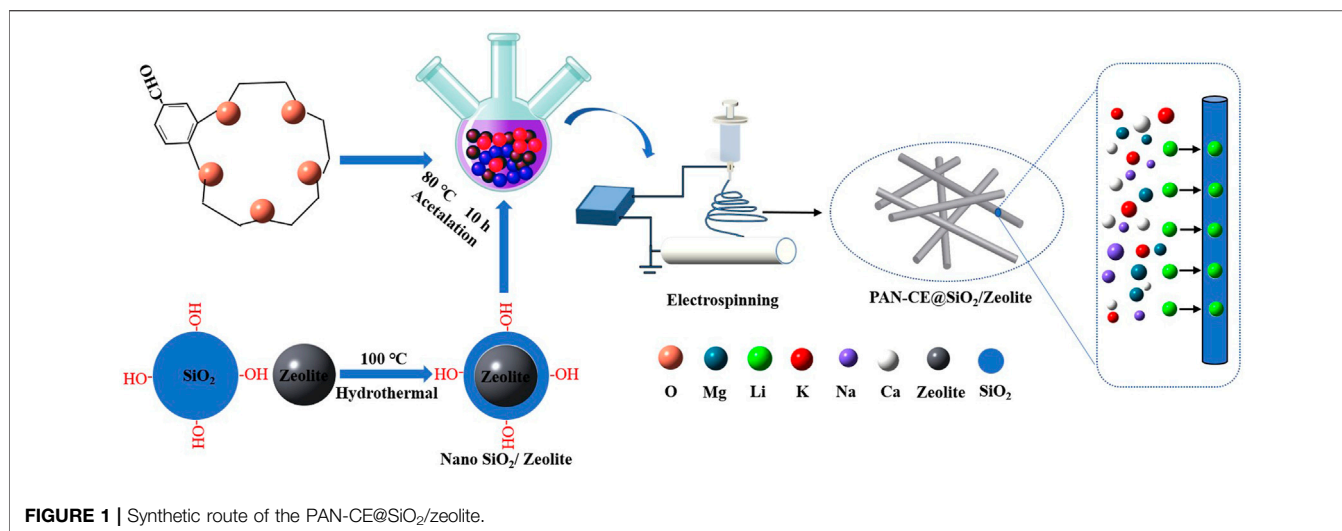
(Kesler et al., 2012). However, it has been confirmed that more than 60% of global lithium resources occur in salt lakes (Song et al., 2017; Liu et al., 2019), so the selective recovery of Li(I) from the salt lake brine is of important economic and environmental significance.

There are several technologies available for selectively separating Li(I) in the salt-lake brine, like the precipitation method (Zhang et al., 2019; Pramanik et al., 2020), solvent extraction method (Shi et al., 2016; Shi et al., 2019; Zhou et al., 2021), and adsorption method (Xiao et al., 2013; Marthi and Smith, 2019; Ding et al., 2021; Zhang et al., 2021). Our research group has devoted to research on Li(I) recovery from salt lakes since 2000 and was the first to propose the method of salinity gradient solar ponds for separation of Li(I) from the brine of Zabuye Salt Lake in Tibet Autonomous Region, China. In addition, the first production base in China for lithium ores from the salt lake has been built there, which continues to produce lithium ores so far (Nie et al., 2010, 2011; Yu et al., 2015; Ding et al., 2022). However, the method remains to be further improved because it needs to construct large areas of salt pans and has a long production cycle. To this end, our research group attempted to use the adsorption method to improve the production of Zabuye Salt Lake, because of the simple production processes, costs low, and consumes less energy of the adsorption methods. Attributed to these advantages, the method has received more attention in the separation and recovery of lithium resources from the salt-lake brine (Zhang et al., 2010; Hong et al., 2017). Using the sol-gel method and taking $\text{Ti}(\text{OC}_4\text{H}_9)_4$ and CH_3COOLi as raw materials, Zhang et al. (2016) prepared an ion-sieve precursor Li_2TiO_3 . Through the analyses of Langmuir and Freundlich models, they found that the optimal calcination temperature is approximately 650°C and the elution rate of lithium reach 78.9% after elution with 0.25 mol/L hydrochloric acid (HCl) at 70°C for 8 h, with a dissolution-loss rate of titanium of only 0.07%. Then, a foaming agent is prepared using zeolite, talcum powder, and alumina as raw materials, which improves the fluidity and permeability of the ionic sieve. After elution with HCl for 24 h, the saturated adsorption capacity for Li(I) reaches 21.0 mg/g (Zhang et al., 2016). To enlarge the specific area of the sorbent, some researchers prepared H_2TiO_3 as nanotubes by hydrothermal method, which increases the adsorption capacity by 5%–10% and enables the maximum adsorption capacity of 39.43 mg/g (Moazeni et al., 2015). Manganese-based adsorbing materials (e.g. HMn_2O_4 , $\text{H}_{1.6}\text{Mn}_{1.6}\text{O}_4$, and $\text{H}_4\text{Mn}_5\text{O}_{12}$) exert specific adsorption effects on Li(I) due to their spinel structures. It is reported that the maximum adsorption capacity of this type of adsorbing material can reach 40 mg/g, and in the mixed solution, the metal ions Li(I), Mg(II), Ca(II), K(I), and Na(I) are listed in a descending order in accordance with their distribution coefficients K_d . Therefore, these materials are applicable to separation of Li(I) in mixed solution (Feng et al., 1993; Robinson et al., 2010; Xiao et al., 2015; Gao et al., 2018). Hong et al. (2015) separately used chitosan and alpha-alumina bead (AAB) as the binder of $\text{Li}_{1.33}\text{Mn}_{1.67}\text{O}_4$ particles, which impart stable structures to granulated adsorbing materials, and the adsorption capacity only decreases by 2% after 14 cycles. To further improve the

recovery rate of the adsorbing materials in geothermal water, Paranthaman et al. (2017) applied a three-step synthesis method and a bench-scale column extraction setup to increase the recovery rate of the adsorbing material to 91%. Meanwhile, the selectivity coefficient for Li(I) is 47.8 and 212 higher than those for Na(I) and K(I), respectively, allowing efficient selective separation of Li(I). It is evident that some researchers have extensively studied the structural stability, adsorption capacity, and recovery of adsorbing materials. However, these sorbents are entire particles or powders, which encounter large flow resistance in the adsorption process and may be crushed, thus decreasing the industrial utilization rate of the adsorbing materials. Therefore, it is an important research direction to develop a highly permeable and segregative adsorbing material of a high recovery rate.

Fiber-based adsorbing materials encounter low flow resistance and exhibit excellent mass transfer performance in the dynamic adsorption process, so they are deemed as ideal industrial adsorbing materials. According to the electrospinning technology, Koushkbaghi et al. (2018) prepared a dual-layer mixed matrix membrane to separate Cr(VI) and Pb(II) in sewage. Besides, they determined that the adsorption capacities for Cr(VI) and Pb(II) are 509.7 and 525.8 mg/g at pH of 2 and room temperature under the optimal separation conditions, basically remaining unchanged after three cycles. In order to increase the adsorption sites of polyacrylonitrile (PAN) fibers, some scholars performed phosphorylation and grafting on the prepared PAN fibers, and the grafting amount of phosphate radicals is 5.45 mg/g after modification. The phosphorylated fibers are found to have an adsorption capacity for Pb(II) being 16.28 mg/g larger than the aminated fibers, and their adsorption performance hardly decreases after four cycles (Zhao et al., 2015). Haider and Park (2009) prepared nanofibers with a diameter of 235 nm using trifluoroacetic acid and chitosan, whose adsorption capacities for Pb(II) and Cu(II) in sewage are separately 263.15 and 485.44 mg/g. The adsorption capacity of such chitosan fibers is 6 and 11 times larger than those of the chitosan microspheres and the raw chitosan, respectively, indicative of the advantage of fiber-based adsorbing materials in adsorption. This indicates that the fiber-based adsorbing materials are of strong adsorbability and a promising industrial application prospect. To our knowledge, there are few reports on separation of Li(I) in salt lakes using fiber-based adsorbing materials. The current research used the chemical grafting and electrospinning technologies and took zeolite as the carrier to graft 4-formoxylbenzo-15-crown-5-ether (4-FB15C5) onto the surface of zeolite. The synthesized nanofibers are used for directional capture of Li(I) in salt lakes.

The mobility and selectivity of the adsorbing materials are critical for the adsorption of Li(I) from the salt lakes. Based on the previous work, the low-cost zeolite was used as the carrier. Through the one-step acetalation, 4-FB15C5 was grafted onto zeolite and the bulk phases of synthesized nano-particles and PAN were blended according to a certain ratio, to prepare the nanofibers. The adsorption mechanism was revealed through the



characterization, adsorption experiments, and theoretical calculation of the prepared adsorbing material. It provides a new idea for the selective separation of Li(I) from the salt lake.

MATERIALS AND METHODS

Materials and Chemicals

The chemical reagents (all analytically pure) used in the research were mainly purchased from Sinopharm Chemical Reagent Co., Ltd. and Rhawn Reagent Co., Ltd. The detailed information of these reagents is given in the Supporting Information (**Supplementary Text S1**). The salt lake brine used was collected from Zabuye Salt Lake and measured to have a pH value of 7.8. The concentrations of various elements were detected using the inductively coupled plasma-atomic emission spectroscopy (ICP-AES) and the results are listed in the Supporting Information (**Supplementary Table S1**).

Nanofibers Synthesized by Grafting Crown Ether on Zeolite

Hexadecyl trimethyl ammonium chloride (1.2 g) and ammonia water (4.5 ml) were added in 50 ml deionized water. After stirring the mixture for 10 min, 4.8 ml tetraethyl orthosilicate, 4 g of zeolite, and 1 g of SiO₂ were added, followed by further stirring for 2 h. The resulting solution was poured in a high-pressure reactor to allow reaction for 2 h. The obtained solid product was calcined for 4 h at 600°C. In this way, zeolite which carried hydroxyl radicals (SiO₂/zeolite) was attained. SiO₂/zeolite of 0.5 g was dissolved in dimethyl sulfoxide, in which 4-formyl benzo 15-crown-5 ether (4-FB15C5) and the catalyst were also added to perform acetalation on the p-toluene sulfonic acid. After reaction at 80°C for 10 h, ethanol was used as the extractant for extraction for 12 h. After being dried, the crown ether (CE) grafted zeolite (CE@SiO₂/zeolite) was attained.

Pretreated CE@SiO₂/zeolite nano-powders of 0.5 g were added in N,N-dimethylformamide. The mixture was subjected to

ultrasonic dispersion for 30 min and then added with polyacrylonitrile (PAN) fibers. After magnetically stirring the mixture at 90°C for 4 h, the uniform and transparent spinning solution with the concentration of 13 wt% was prepared. The spinning solution was poured in a 10 ml needle syringe, for which a 18G needle with an inner diameter of 0.83 mm was used as the spinning head. The syringe was then mounted on a micropump that controlled the flow speed of the spinning solution. The spinning was performed under the following parameters: the voltage, flow speed of spinning solution, rotation speed of the drum receiver, and the receiving distance were 15 kV, 0.25 ml/min, 450 rpm, and 15 cm, respectively. The spinning product was placed in an oven to be dried in vacuum at 50°C for 12 h. As a result, the polyacrylonitrile - crown ether@SiO₂/zeolite (PAN-CE@SiO₂/zeolite) nanofibers were attained, and the synthetic route is illustrated in **Figure 1**.

Characterization

The samples were characterized in each stage of the synthesis and adsorption experiments using technologies including scanning electron microscopy (SEM), X-ray photoelectron spectroscopy (XPS), and Fourier transform infrared (FT-IR) spectrometry. In the adsorption experiment, the ICP-AES was adopted for measurement of ion concentrations in the solution. The specifications of the characterization devices are listed in Supporting Information (**Supplementary Text S2**).

Adsorption Experiment

The static adsorption experiment was conducted to explore the adsorption kinetics of PAN-CE@SiO₂/zeolite for Li(I), adsorption isotherms, and influences of pH values on the adsorption capacity for Li(I). The fixed-bed adsorption method was used to study the recycling performance of PAN-CE@SiO₂/zeolite and its desorption capacity for Li(I). A series of experiments were conducted to investigate the selective adsorption of PAN-CE@SiO₂/zeolite for ions in the salt lake brine. The detailed information is given in Supporting Information (**Supplementary Text S3**).

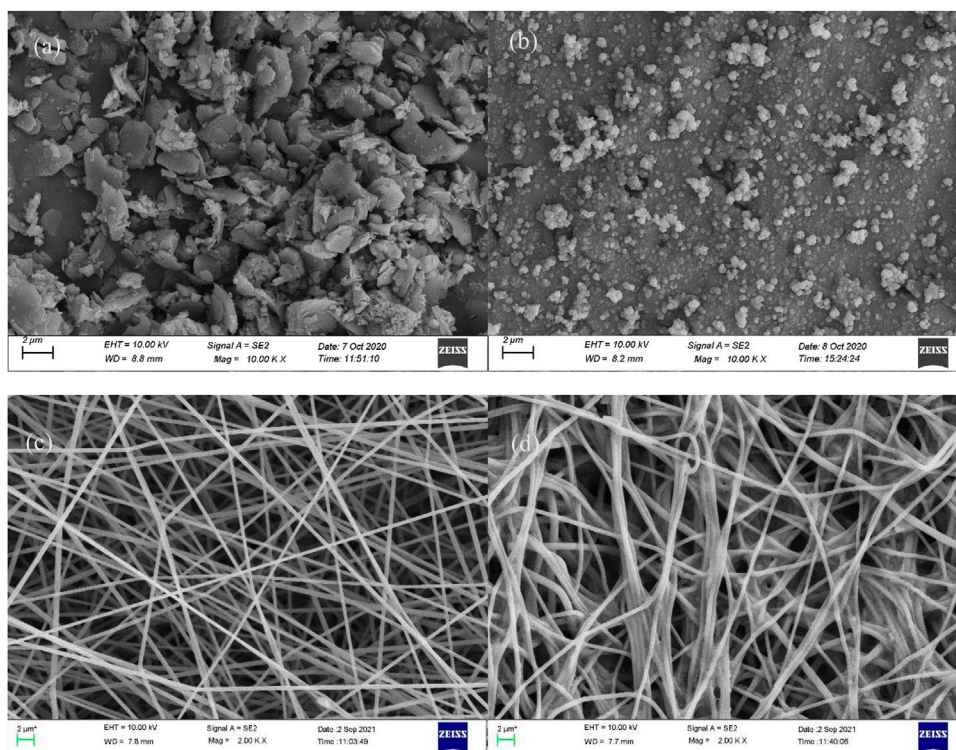


FIGURE 2 | SEM images in different stages. [(A) Zeolite; (B) $\text{SiO}_2/\text{zeolite}$; (C) PAN-CE@ $\text{SiO}_2/\text{zeolite}$ nanofibers; (D) PAN-CE@ $\text{SiO}_2/\text{zeolite}$ nanofibers after adsorbing Li(I)].

Calculation Methods

The Gaussian 09 software and the density functional theory (DFT), combined with results of a series of characterization methods, were used to further explain the adsorption mechanism of PAN-CE@ $\text{SiO}_2/\text{zeolite}$ for Li(I). Due to the reliability of the B3LYP hybrid functional in processing electron exchange and correlation in extensive molecular systems, the 6-31+G (d, p) basis sets of the B3LYP hybrid functional (Ramos-Sanchez et al., 2014) were utilized to optimize the initial structures of complexes of PAN-CE@ SiO_2 and Li(I). Besides, the natural bond orbit (NBO) of the complex was calculated using the 6-311+G (d, p) basis sets of the B3LYP hybrid functional, to further analyze the interaction mechanism between functional groups in PAN-CE@ $\text{SiO}_2/\text{zeolite}$ and Li(I). More details are shown in Supporting Information (Supplementary Text S4).

RESULTS AND DISCUSSION

Characterization

It can be seen from **Figure 2A** that there are original liminated structures in the zeolite. **Figure 2B** shows the nano-particles formed by wrapping zeolite with silicone, displaying that the liminated structures in **Figure 2A** have disappeared, and the particles have smooth surface and uniform sizes. This indicates

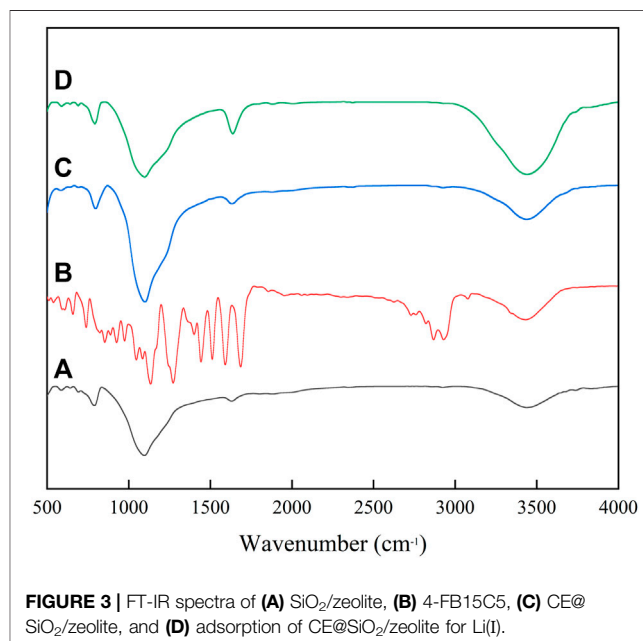


FIGURE 3 | FT-IR spectra of (A) $\text{SiO}_2/\text{zeolite}$, (B) 4-FB15C5, (C) CE@ $\text{SiO}_2/\text{zeolite}$, and (D) adsorption of CE@ $\text{SiO}_2/\text{zeolite}$ for Li(I).

that SiO_2 has successfully wrapped zeolite particles and hydroxy has been introduced. The nanofibers in **Figure 2C** have regular morphologies, a uniformly distributed diameter of about 400 nm,

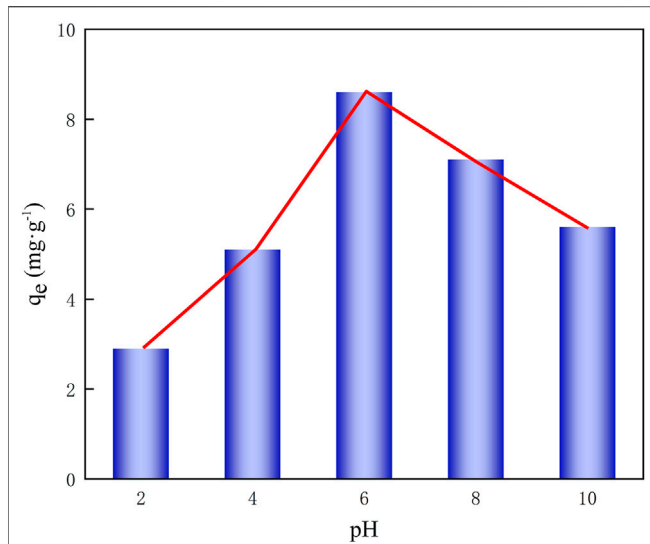


FIGURE 4 | Influences of the pH value on the adsorption capacity of PAN-CE@SiO₂/zeolite for Li(I).

TABLE 1 | Adsorption performance of sorbents for Li(I) in other research.

Sorbents	Adsorption equilibrium time (h)	Ref
PAN-CE@SiO ₂ /zeolite	2.5	Current research
Li/Al-LDHs	24	Sun et al. (2019)
Li ₂ TiO ₃	24	Chitrakar et al. (2014)
Li ₄ Mn ₅ O ₁₂	10	Xiao et al. (2015)
Li _{1.6} Mn _{1.6} O ₄	24	Gao et al. (2018)

TABLE 2 | Kinetics parameters.

Pseudo-first-order			Pseudo-second-order		
k1 (min ⁻¹)	qe, cal (mg/g)	R12	k2 (mg/(g·min))	qe, cal (mg/g)	R2 ²
0.041	2.1	0.968	0.021	2.4	0.993

and smooth surface. In addition, there is large space between these nanofibers. All of these are beneficial for PAN-CE@SiO₂/zeolite to capture target ions in the salt-lake brine.

Figure 3 illustrates the FT-IR spectra of SiO₂/zeolite, 4-FB15C5, CE@SiO₂/zeolite, and adsorption of CE@SiO₂/zeolite for Li(I). An antisymmetric stretching vibration absorption peak of Si-O-Si occurs at 1,083 cm⁻¹ in **Figures 3A,C,D**, which is attributed to SiO₂ in the zeolite carrier (Sileika et al., 2011; Salih et al., 2015). In **Figure 3B**, the peak at 1,681 cm⁻¹ is an absorption peak of aldehyde groups in CE monomers, and there is an obvious stretching vibration absorption peak of epoxy groups in CE at 590 cm⁻¹. The absorption peak of aldehyde groups at 1,681 cm⁻¹ in **Figure 3B** disappears in **Figure 3C** after acetalation, while the characteristic absorption peak of C-O- at 590 cm⁻¹ still persists (Li et al., 2015; Huang et al., 2018). The result shows that 4-FB15C5 has been successfully grafted on SiO₂/zeolite, that is, CE@SiO₂/zeolite has been synthesized.

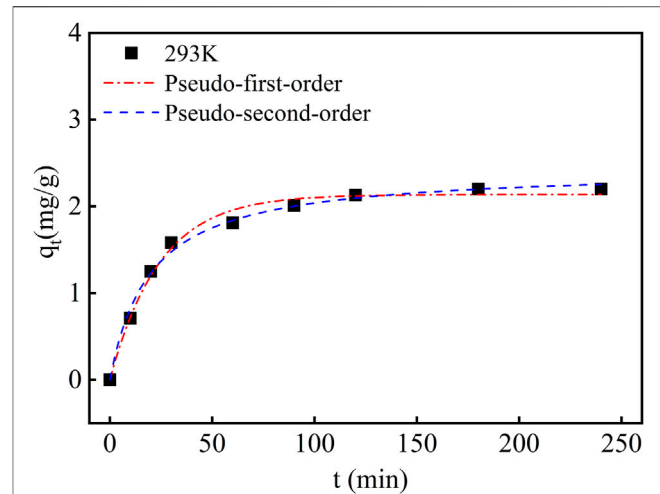


FIGURE 5 | Curves of the adsorption kinetics of PAN-CE@SiO₂/zeolite.

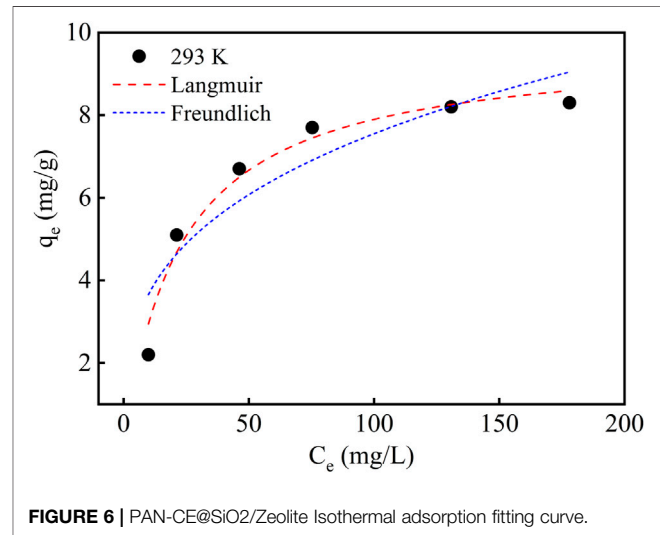
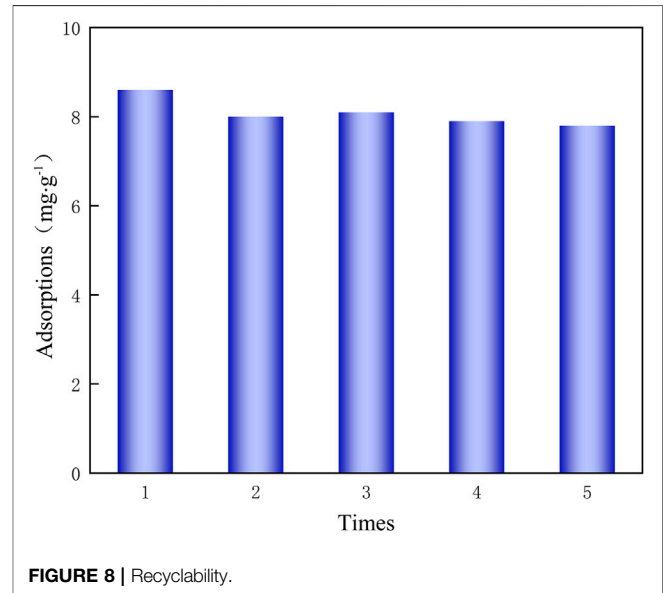
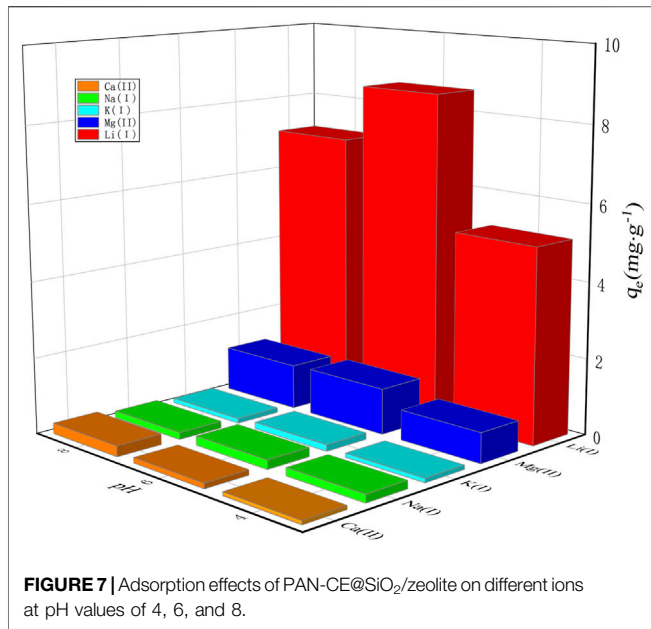


FIGURE 6 | PAN-CE@SiO₂/Zeolite Isothermal adsorption fitting curve.

Adsorption Behaviors

The pH value may change existence forms of metal ions in solution and affects the loads of surface charges of materials. Considering this, the pH value was set from 2 to 10 to study its influences on the adsorption of PAN-CE@SiO₂/zeolite for Li(I). **Figure 4** shows that the curve of the adsorption capacity is low in both sides and high in the middle, and the adsorption capacity maximizes at a pH value of 6 and it reduces either increase or decrease from the value. This is because under a low pH value, the epoxy groups are protonated, so that they carry lots of positive charges and show an increasing repulsive force to Li(I). As the pH value increases from 2 to 6, the protonation of epoxy groups weakens and effective adsorption sites increase, which results in a larger adsorption capacity for Li(I). When the pH value is greater than 6, the adsorption capacity decreases, possibly related to the combination of OH⁻ in the solution with Li(I) to form compounds of negative valence states. As oxygen in the epoxy groups also has a negative valence state, they are relatively



repulsive to the compounds and therefore the adsorption capacity constantly decreases when the pH value exceeds 6.

Figure 5 shows the fitting curves of the adsorption kinetics of PAN-CE@SiO₂/zeolite with models. As shown in this figure, the adsorption rate remain high in the first 2 h, while it decreases thereafter and basically reaches equilibrium in 2.5 h. This is because Li(I) has a high concentration in the initial solution. At the beginning, plenty of adsorption sites are present on PAN-CE@SiO₂/zeolite, contributing to easy capture of Li(I) in the solution. After numerous adsorption sites on the surface of PAN-CE@SiO₂/zeolite are occupied, the adsorption rate slows down; after all adsorption sites are occupied, the desorption and adsorption reach a dynamic equilibrium at which the adsorption capacity does not change obviously any longer. The PAN-CE@SiO₂/zeolite prepared in the research adsorbs Li(I) faster than adsorbing materials reported elsewhere (**Table 1**), indicating that adsorption sites on epoxy groups are more identifiable, so the adsorbing material is of advantages in industrial application.

The adsorption kinetics is an important factor influencing the adsorption performance. In the research, the pseudo-first-order and pseudo-second-order kinetic models were used to analyze the adsorption data, so as to investigate the adsorption mechanism. **Table 2** lists the kinetics parameters. From **Table 2**, the pseudo-second-order kinetic model has a larger correlation coefficient than the pseudo-first-order kinetic model, reaching 0.993, and yields an equilibrium adsorption capacity more approximated to

the actual one. Therefore, the adsorption can be deemed as a chemical adsorption process.

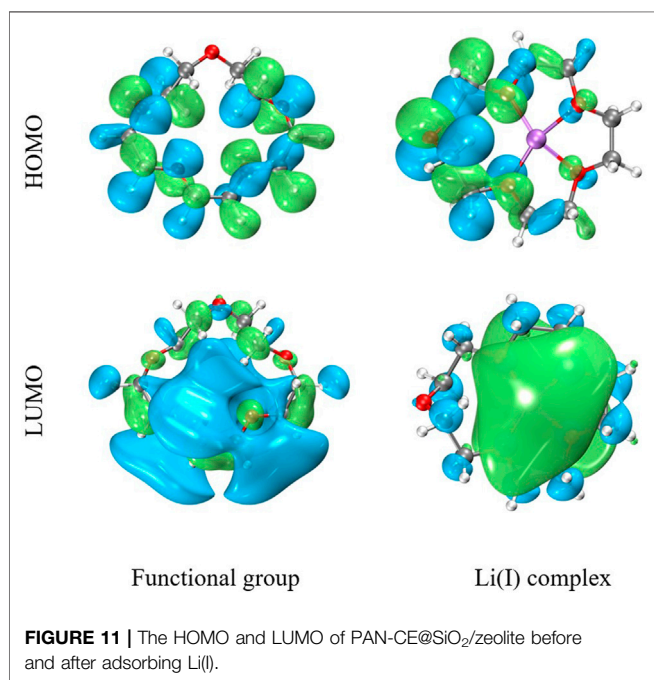
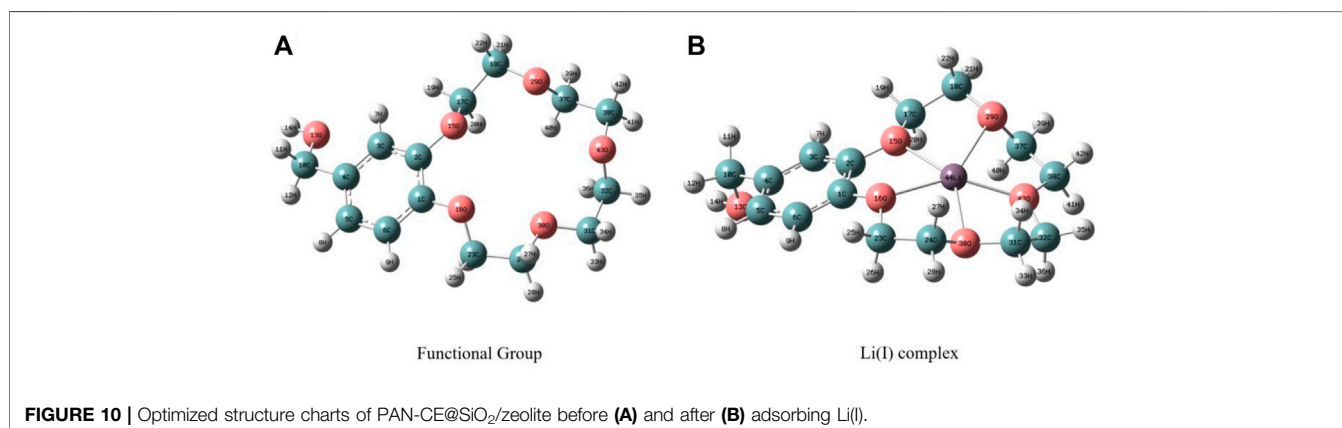
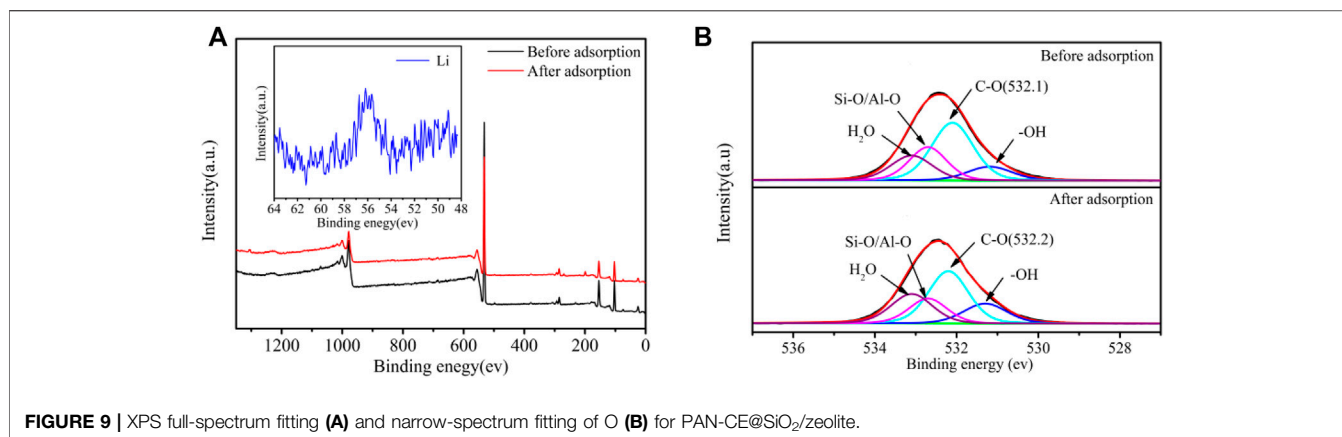
In this study, Freundlich and Langmuir isothermal adsorption models were used to fit the experimental data. The fitting curves are shown in **Figure 6** and the relevant data are listed in **Table 3**. The adsorption capacity constantly increases with the rising concentration of Li(I) in the solution. As the Li(I) concentration rises to 150 mg/L, the adsorption capacity does not enlarge with the concentration any longer. This is because the adsorption sites of PAN-CE@SiO₂/zeolite come from the epoxy groups in CE. At the beginning, the mass transfer driving force is enhanced as the Li(I) concentration rises in the solution. However, the adsorption sites in the epoxy groups have a fixed number and after they are basically completely occupied by Li(I), the adsorption capacity will not change apparently any longer. It can be seen from **Figure 6** that the Langmuir isothermal adsorption model is more suitable for describing the adsorption process, because the maximum adsorption capacity calculated thereby is approximated to that obtained in the experiment. The result reveals that the adsorption process can be regarded as monolayer adsorption and there is no interaction between epoxy groups in the adsorbing material.

Selectivity and Regenerability

The selectivity and recyclability of adsorbing materials are important factors for judging whether they are suitable for industrial application or not. In the salt lake brine, Li(I) is

TABLE 3 | Parameters of Langmuir and Freundlich models.

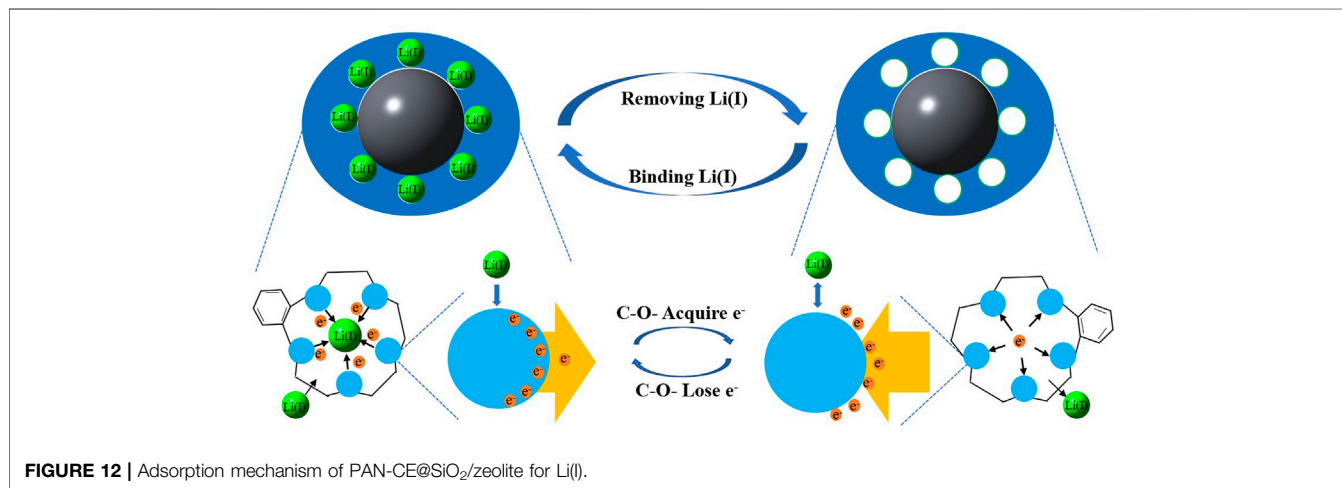
Temperature (K)	$q_{e, \text{exp}}$ (mg/g)	Langmuir			Freundlich		
		q_m, cal (mg/g)	KL (L/mg)	R12	1/n	KF (mg/g)	R_2^2
298	8.2	8.6	0.045	0.959	3.190	1.782	0.816



generally associated with alkali metal ions Na(I) and K(I) as well as alkali-earth metal ions Mg(II) and Ca(II). Considering this, these four metal ions were added in the solution to study the selectivity of PAN-CE@SiO₂/zeolite for Li(I) through the competitive adsorption. **Figure 7** shows the adsorption capacities of PAN-CE@SiO₂/zeolite for different ions at pH values of 4, 6, and 8, and the parameters of competitive adsorption are listed in Supporting Information (**Supplementary Table S2**). As shown in the figure, PAN-CE@SiO₂/zeolite exhibits a significant adsorption effect on Li(I), and also adsorbs a little amount of Mg(II), while it hardly adsorbs Na(I), Ca(II), and K(I). These ions are ranked in a descending order as Li(I), Mg(II), Na(I), Ca(II), and K(I) according to their competitive adsorption and the adsorption capacities are maximized at a pH value of 6, which is in line with the analysis results of influences of pH values on the adsorption. This is possibly because there is numerous H⁺ in the solution at a pH value of 4 to coordinate with C-O- structures in epoxy groups of PAN-CE@SiO₂/zeolite, thus affecting the Li(I) adsorption. Because Mg(II) has a radius (0.065 nm) approximated to that of Li(I) (0.068 nm), PAN-CE@SiO₂/zeolite also adsorbs certain Mg(II).

TABLE 4 | The calculated parameters for the complex.

Complex	Interaction energy (kcal/mol)	NBO partial charge		M(II) electron configuration	E (2) energy(kcal/mol)				
		Ligand	M(I)		LP(O15)-LP*(M)	LP(O16)-LP*(M)	LP(O29)-LP*(M)	LP(O30)-LP*(M)	LP (O43)-LP*(M)
Li(I) complex	-62.75	0.719	0.421	$2s^{0.09}3p^{0.18}3d^{0.01}$	1.33	9.21	11.26	8.92	11.54



After adsorption using PAN-CE@SiO₂/zeolite, 0.5 M HCl was used for desorption. Through five adsorption-desorption cycles (Figure 8), PAN-CE@SiO₂/zeolite still exhibits an adsorption capacity of 7.8 mg/g for Li(I), so the material can be recycled.

Adsorption Mechanism

The SEM image of PAN-CE@SiO₂/zeolite after adsorbing Li(I) is illustrated in Figure 2D. Compared with Figure 2C, the nanofibers in Figure 2D are obviously thicker and there are coarse particles thereon. This is possibly because Li(I) enters the nanofibers to coordinate with epoxy groups changing the location of O atoms in the epoxy groups, causing the nanofibers to expand. At the same time, the change of the permeation pressure thickens the nanofibers and the adsorbed metal ions result in the coarse surface. Figures 3C,D separately show the IF spectra of CE@SiO₂/zeolite before and after adsorbing Li(I). After adsorbing Li(I), the C-O- absorption peak in the epoxy structure in CE at 590 cm⁻¹ shifts to 588 cm⁻¹, a result of the energy transfer needed in the coordination of C-O- and Li(I), so that the stretching vibration absorption peak of epoxy groups shifts (Sileika et al., 2011; Huang et al., 2018). Figures 9A,B depict the XPS full-spectrum fitting and narrow-spectrum fitting of PAN-CE@SiO₂/zeolite before and after adsorbing Li(I). After adsorbing Li(I), a new characteristic peak appears on the full-spectrum fitting curve at 55.84 eV, which is attributed to Li(I) coordinated with C-O-. Figure 9B illustrates the peak fitting of C-O- before and after Li(I) adsorption. After adsorption, the C-O- characteristic peak shifts from 532.1 to 532.2 eV (Xu et al., 2020), possibly because O in C-O- as the electron donor is involved in the adsorption for Li(I).

To further explore the adsorption mechanism of PAN-CE@SiO₂/zeolite for Li(I), the DFT was used to compute the optimal structures of functional groups on the surface of PAN-CE@SiO₂/zeolite, as illustrated in Figure 10. The computation parameters can refer to Supporting Information (Supplementary Table S2).

The optimized structure charts show that Li(I) is located at the center of the epoxy groups. This is because the epoxy groups of CE and Li(I) complex show the minimum vacancy size of 4.72 Å, while the sum of diameters of Li(I) and O²⁻ ions is 3.94 Å, so the vacancy of the epoxy functional groups can just accommodate Li(I) in the coordination process.

Table 4 shows the parameters for calculating the NBO. It can be seen from the table that the binding energy of the Li(I) complex is -62.75 kcal/mol, indicative of strong affinity of PAN-CE@SiO₂/zeolite for Li(I). According to the analysis of NBO partial charge, Li(I) and its ligand have charged by 0.421 and 0.719 eV, respectively. This suggests the appearance of electron transfer between the surface functional groups and metal ions in the adsorption process. Li(I) displays a natural electron configuration of $2s^{0.09}3p^{0.18}3d^{0.01}$, which means that electrons mainly transfer from functional groups to the 3p orbit of Li(I), corresponding to the XPS fitting results as shown in Figure 9. That is, C-O- in the epoxy groups of PAN-CE@SiO₂/zeolite as electron donors participate in the coordination of Li(I). Figure 11 illustrates the highest occupied molecular orbit (HOMO) and lowest unoccupied molecular orbit (LUMO) of PAN-CE@SiO₂/zeolite before and after adsorbing Li(I), from which is seen that the HOMO and LUMO both change after Li(I) adsorption compared with

those before. This further confirms that the electron transfer between the ligand and metal ions in the adsorption process. Meanwhile, the stabilization energy $E(2)$ reflects the degree of delocalization of electrons according to analysis of the second-order perturbation theory. As listed in **Table 4**, the stabilization energies $E(2)$ of LP(O)-LP*(Li) for Li(I) are 1.33, 9.21, 11.26, 8.92, and 11.54 kcal/mol separately. This reveals the electron transfer between the five O atoms in PAN-CE@SiO₂/zeolite and Li(I), thus leading to the coordination and the formation of stable complexes. The result agrees with the XPS and FT-IR results. As a result, the five O atoms in epoxy groups as electron donors coordinate with Li(I), reaching the goal of selective capture of Li(I) in the salt-lake brine. Combining the adsorption experiment, the series of characterization, and DFT calculation, the adsorption mechanism is described in **Figure 12**.

CONCLUSION

4-FB15C5 was grafted on zeolite through acetalation to form a kind of nanofiber PAN-CE@SiO₂/zeolite containing CE. Leveraging the specific vacancies of epoxy groups in CE and their binding force for Li(I), Li(I) was directionally captured, thus realizing the selective separation of Li(I) in the salt lake. PAN-CE@SiO₂/zeolite reached adsorption equilibrium after 2.5 h and its maximum adsorption capacity was 8.6 mg/g. After 5 adsorption-desorption cycles, the adsorption capacity could maintain at 7.8 mg/g, suggesting favorable stability and strong regeneration ability. The stabilisation energies $E(2)$ of LP(O)-LP*(Li) for Li(I) are 1.33, 9.21, 11.26, 8.92, and 11.54 kcal/mol separately. Through use of FT-IR, SEM, and XPS and combining with DFT calculation, the adsorption mechanism of PAN-CE@SiO₂/zeolite for Li(I) is revealed. The results indicate that after dsp^3 hybridization of the outer orbit 2s of Li(I), the outer electrons of the nanofiber containing zeolite carrier and CE

REFERENCES

- Berecibar, M. (2019). Machine-learning Techniques Used to Accurately Predict Battery Life. *Nature* 568 (7752), 325–326. doi:10.1038/d41586-019-01138-1
- Chitrakar, R., Makita, Y., Ooi, K., and Sonoda, A. (2014). Lithium Recovery from Salt Lake Brine by H₂TiO₃. *Dalton Trans.* 43 (23), 8933–8939. doi:10.1039/C4DT00467A
- Ding, T., Wu, Q., Zheng, M., Nie, Z., Li, M., Peng, S., et al. (2021). Polyacrylonitrile/Crown Ether Composite Nanofibres with High Efficiency for Adsorbing Li(I): Experiments and Theoretical Calculations. *Front. Energy Res.* 9, 765612. doi:10.3389/fenrg.2021.765612
- Ding, T., Zheng, M., Nie, Z., Ma, L., Ye, C., Wu, Q., et al. (2022). Impact of Regional Climate Change on the Development of Lithium Resources in Zabuye Salt Lake, Tibet. *Front. Earth Sci.* 10, 865158. doi:10.3389/feart.2022.865158
- Feng, Q., Miyai, Y., Kanoh, H., and Ooi, K. (1993). Lithium(1+) and Magnesium(2+) Extraction and Lithium(1+) Insertion Reactions with Lithium Magnesium Manganese Oxide (LiMg_{0.5}Mn_{1.5}O₄) Spinel in the Aqueous Phase. *Chem. Mat.* 5 (3), 311–316. doi:10.1021/cm00027a013
- Gao, A., Sun, Z., Li, S., Hou, X., Li, H., Wu, Q., et al. (2018). The Mechanism of Manganese Dissolution on Li_{1.6}Mn_{1.6}O₄ Ion Sieves with HCl. *Dalton Trans.* 47 (11), 3864–3871. doi:10.1039/C8DT00033F

mainly migrate to the orbit to coordinate with Li(I), thus realizing the capture of Li(I). PAN-CE@SiO₂/zeolite can be used to selectively recover Li(I) from the salt lake brine, and therefore is an adsorbing material of a promising application prospect.

DATA AVAILABILITY STATEMENT

The original contributions presented in the study are included in the article/**Supplementary Material**, further inquiries can be directed to the corresponding authors.

AUTHOR CONTRIBUTIONS

TD major write up and review; MZ and SP conception, outline, and review; YL, QW and ZN critical review, content suggestions, and proofreading.

ACKNOWLEDGMENTS

The authors gratefully thank the Joint Funds of the National Natural Science Foundation of China (Research Project No. U21A2017) and the National Natural Science Foundation of China for financial support (Research Project No. U20A20148; 91962219).

SUPPLEMENTARY MATERIAL

The Supplementary Material for this article can be found online at: <https://www.frontiersin.org/articles/10.3389/fenrg.2022.895681/full#supplementary-material>

- Haider, S., and Park, S.-Y. (2009). Preparation of the Electrospun Chitosan Nanofibers and Their Applications to the Adsorption of Cu(II) and Pb(II) Ions from an Aqueous Solution. *J. Membr. Sci.* 328 (1-2), 90–96. doi:10.1016/j.memsci.2008.11.046
- Hong, H.-J., Park, I.-S., Ryu, J., Ryu, T., Kim, B.-G., and Chung, K.-S. (2015). Immobilization of Hydrogen Manganese Oxide (HMO) on Alpha-Alumina Bead (AAB) to Effective Recovery of Li⁺ from Seawater. *Chem. Eng. J.* 271, 71–78. doi:10.1016/j.cej.2015.02.023
- Hong, H. J., Ryu, T., Park, I. S., Kim, M., Shin, J., Kim, B. G., et al. (2017). Highly Porous and Surface-Expanded Spinel Hydrogen Manganese Oxide (HMO)/Al₂O₃ Composite for Effective Lithium (Li) Recovery from Seawater. *Chem. Eng. J.* 337, 455–461. doi:10.1016/j.cej.2017.12.130
- Huang, W., Liu, S., Liu, J., Zhang, W., and Pan, J. (2018). 2-Methylol-12-crown-4 Ether Immobilized PolyHIPES toward Recovery of Lithium(I). *New J. Chem.* 42 (20), 16814–16822. doi:10.1039/C8NJ01961D
- Jiménez-de-la-Cuesta, D., and Mauritsen, T. (2019). Emergent Constraints on Earth's Transient and Equilibrium Response to Doubled CO₂ from Post-1970s Global Warming. *Nat. Geosci.* 12 (11), 902–905. doi:10.1038/s41561-019-0463-y
- Johnson, G. C., and Lyman, J. M. (2020). Warming Trends Increasingly Dominate Global Ocean. *Nat. Clim. Chang.* 10 (8), 757–761. doi:10.1038/s41558-020-0822-0

- Kesler, S. E., Gruber, P. W., Medina, P. A., Keoleian, G. A., Everson, M. P., and Wallington, T. J. (2012). Global Lithium Resources: Relative Importance of Pegmatite, Brine and Other Deposits. *Ore Geol. Rev.* 48, 55–69. doi:10.1016/j.oregeorev.2012.05.006
- Koushkbaghi, S., Zakialamdari, A., Pishnamazi, M., Ramandi, H. F., Aliabadi, M., and Irani, M. (2018). Aminated-Fe₃O₄ Nanoparticles Filled chitosan/PVA/PES Dual Layers Nanofibrous Membrane for the Removal of Cr(VI) and Pb(II) Ions from Aqueous Solutions in Adsorption and Membrane Processes. *Chem. Eng. J.* 337, 169–182. doi:10.1016/j.cej.2017.12.075
- Lee, J., Kitchaev, D. A., Kwon, D.-H., Lee, C.-W., Papp, J. K., Liu, Y.-S., et al. (2018). Reversible Mn²⁺/Mn⁴⁺ Double Redox in Lithium-Excess Cathode Materials. *Nature* 556 (7700), 185–190. doi:10.1038/s41586-018-0015-4
- Li, T. L., Pei, H. C., Yuan, W. J., Yan, F., Li, J. X., He, B. Q., et al. (2015). Preparation and Characterization of Polyvinyl Alcohol Copolymer Grafted with 4'-Formoxybenzo-15-Crown-5-Ether for Lithium Isotopes Separation. *Acta Polym. Sin.* 7, 792–799.
- Liu, G., Zhao, Z., and Ghahreman, A. (2019). Novel Approaches for Lithium Extraction from Salt-Lake Brines: A Review. *Hydrometallurgy* 187, 81–100. doi:10.1016/j.hydromet.2019.05.005
- Marthi, R., and Smith, Y. R. (2019). Selective Recovery of Lithium from the Great Salt Lake Using Lithium Manganese Oxide-Diatomaceous Earth Composite. *Hydrometallurgy* 186, 115–125. doi:10.1016/j.hydromet.2019.03.011
- Moazeni, M., Hajipour, H., Askari, M., and Nusheh, M. (2015). Hydrothermal Synthesis and Characterization of Titanium Dioxide Nanotubes as Novel Lithium Adsorbents. *Mater. Res. Bull.* 61, 70–75. doi:10.1016/j.materresbull.2014.09.069
- Nie, Z., Bu, L., Zheng, M., and Huang, W. (2011). Experimental Study of Natural Brine Solar Ponds in Tibet. *Sol. Energy* 85 (7), 1537–1542. doi:10.1016/j.solener.2011.04.011
- Nie, Z., Bu, L., and Zheng, M. (2010). Phase Chemistry Study on Brine from the Zabuye Carbonate-type Salt Lake in Tibet. *Acta Geol. sin.-engl.* 84 (4), 587–592. doi:10.1017/S0004972710001772
- Paranthaman, M. P., Li, L., Luo, J., Hoke, T., Ucar, H., Moyer, B. A., et al. (2017). Recovery of Lithium from Geothermal Brine with Lithium-Aluminum Layered Double Hydroxide Chloride Sorbents. *Environ. Sci. Technol.* 51 (22), 13481–13486. doi:10.1021/acs.est.7b03464
- Pramanik, B. K., Asif, M. B., Roychand, R., Shu, L., Jegatheesan, V., Bhuiyan, M., et al. (2020). Lithium Recovery from Salt-Lake Brine: Impact of Competing Cations, Pretreatment and Preconcentration. *Chemosphere* 260, 127623. doi:10.1016/j.chemosphere.2020.127623
- Ramos-Sanchez, G., Callejas-Tovar, A., Scanlon, L. G., and Balbuena, P. B. (2014). DFT Analysis of Li Intercalation Mechanisms in the Fe-Phthalocyanine Cathode of Li-Ion Batteries. *Phys. Chem. Chem. Phys.* 16 (2), 743–752. doi:10.1039/C3CP53161A
- Robinson, D. M., Go, Y. B., Greenblatt, M., and Dismukes, G. C. (2010). Water Oxidation by λ -MnO₂: Catalysis by the Cubical Mn₄O₄ Subcluster Obtained by Delithiation of Spinel LiMn₂O₄. *J. Am. Chem. Soc.* 132 (33), 11467–11469. doi:10.1021/ja1055615
- Salih, A., Ahmad, M., Ibrahim, N., Dahlan, K., Tajau, R., Mahmood, M., et al. (2015). Synthesis of Radiation Curable Palm Oil-Based Epoxy Acrylate: NMR and FTIR Spectroscopic Investigations. *Molecules* 20 (8), 14191–14211. doi:10.3390/molecules200814191
- Shi, C., Jing, Y., and Jia, Y. (2016). Solvent Extraction of Lithium Ions by Tri-n-butyl Phosphate Using a Room Temperature Ionic Liquid. *J. Mol. Liq.* 215, 640–646. doi:10.1016/j.molliq.2016.01.025
- Shi, D., Cui, B., Li, L., Peng, X., Zhang, L., and Zhang, Y. (2019). Lithium Extraction from Low-Grade Salt Lake Brine with Ultrahigh Mg/Li Ratio Using TBP - Kerosene - FeCl₃ System. *Sep. Purif. Technol.* 211, 303–309. doi:10.1016/j.seppur.2018.09.087
- Sileika, T. S., Kim, H.-D., Maniak, P., and Messersmith, P. B. (2011). Antibacterial Performance of Polydopamine-Modified Polymer Surfaces Containing Passive and Active Components. *ACS Appl. Mat. Interfaces* 3 (12), 4602–4610. doi:10.1021/am200978h
- Song, J. F., Nghiem, L. D., Li, X.-M., and He, T. (2017). Lithium Extraction from Chinese Salt-Lake Brines: Opportunities, Challenges, and Future Outlook. *Environ. Sci. Water Res. Technol.* 3 (4), 593–597. doi:10.1039/c7ew00020k
- Sun, Y., Guo, X., Hu, S., and Xiang, X. (2019). Highly Efficient Extraction of Lithium from Salt Lake Brine by LiAl-Layered Double Hydroxides as Lithium-Ion-Selective Capturing Material. *J. Energy Chem.* 34, 80–87. doi:10.1016/j.jechem.2018.09.022
- Tarascon, J.-M., and Armand, M. (2001). Issues and Challenges Facing Rechargeable Lithium Batteries. *Nature* 414, 359–367. doi:10.1038/35104644
- Wu, J., Chen, J., Huang, Y., Feng, K., Deng, J., Huang, W., et al. (2019). Cobalt Atoms Dispersed on Hierarchical Carbon Nitride Support as the Cathode Electrocatalyst for High-Performance Lithium-Polysulfide Batteries. *Sci. Bull.* 64 (24), 1875–1880. doi:10.1016/j.scib.2019.08.016
- Xiao, J.-L., Sun, S.-Y., Wang, J., Li, P., and Yu, J.-G. (2013). Synthesis and Adsorption Properties of Li_{1.6}Mn_{1.6}O₄ Spinel. *Ind. Eng. Chem. Res.* 52 (34), 11967–11973. doi:10.1021/ie400691d
- Xiao, J., Nie, X., Sun, S., Song, X., Li, P., and Yu, J. (2015). Lithium Ion Adsorption-Desorption Properties on Spinel Li₄Mn₅O₁₂ and pH-dependent Ion-Exchange Model. *Adv. Powder Technol.* 26 (2), 589–594. doi:10.1016/j.apt.2015.01.008
- Xu, Z., Rong, M., Meng, Q., Yao, H., Ni, S., Wang, L., et al. (2020). Fabrication of Hypercrosslinked Hydroxyl-Rich Solid Phase Extractants for Cesium Separation from the Salt Lake Brine. *Chem. Eng. J.* 400, 125991. doi:10.1016/j.cej.2020.125991
- Yu, J., Zheng, M., Wu, Q., Nie, Z., and Bu, L. (2015). Extracting Lithium from Tibetan Dangxiong Tso Salt Lake of Carbonate Type by Using Geothermal Salinity-Gradient Solar Pond. *Sol. Energy* 115, 133–144. doi:10.1016/j.solener.2015.02.021
- Zhang, G., Zhang, J., Zhou, Y., Qi, G., Zeng, J., Sun, Y., et al. (2021). Practical Synthesis of Manganese Oxide MnO₂·0.5H₂O for an Advanced and Applicable Lithium Ion-Sieve. *J. Solid State Chem.* 293, 121768. doi:10.1016/j.jssc.2020.121768
- Zhang, L., Zhou, D., Yao, Q., and Zhou, J. (2016). Preparation of H₂TiO₃-lithium Adsorbent by the Sol-Gel Process and its Adsorption Performance. *Appl. Surf. Sci.* 368 (apr.15), 82–87. doi:10.1016/j.apsusc.2016.01.203
- Zhang, Q.-H., Li, S.-P., Sun, S.-Y., Yin, X.-S., and Yu, J.-G. (2010). Lithium Selective Adsorption on Low-Dimensional Titania Nanoribbons. *Chem. Eng. Sci.* 65 (1), 165–168. doi:10.1016/j.ces.2009.06.001
- Zhang, Y., Hu, Y., Wang, L., and Sun, W. (2019). Systematic Review of Lithium Extraction from Salt-Lake Brines via Precipitation Approaches. *Miner. Eng.* 139, 105868. doi:10.1016/j.mineng.2019.105868
- Zhao, R., Li, X., Sun, B., Shen, M., Tan, X., and Ding, Y. (2015). Preparation of Phosphorylated Polyacrylonitrile-Based Nanofiber Mat and its Application for Heavy Metal Ion Removal. *Chem. Eng. J.* 268, 290–299. doi:10.1016/j.cej.2015.01.061
- Zhou, W., Li, Z., and Xu, S. (2021). Extraction of Lithium from Magnesium-Rich Solution Using Tri-n-butyl Phosphate and Sodium Hexafluorophosphate. *J. Sustain. Metall.* 7 (3), 1368–1378. doi:10.1007/s40831-021-00430-7

Conflict of Interest: The authors declare that the research was conducted in the absence of any commercial or financial relationships that could be construed as a potential conflict of interest.

Publisher's Note: All claims expressed in this article are solely those of the authors and do not necessarily represent those of their affiliated organizations, or those of the publisher, the editors and the reviewers. Any product that may be evaluated in this article, or claim that may be made by its manufacturer, is not guaranteed or endorsed by the publisher.

Copyright © 2022 Ding, Zheng, Peng, Nie, Lin and Wu. This is an open-access article distributed under the terms of the Creative Commons Attribution License (CC BY). The use, distribution or reproduction in other forums is permitted, provided the original author(s) and the copyright owner(s) are credited and that the original publication in this journal is cited, in accordance with accepted academic practice. No use, distribution or reproduction is permitted which does not comply with these terms.